**SpezialForschungsBereich F 32**

Karl–Franzens Universität Graz
Technische Universität Graz
Medizinische Universität Graz

# Correction of systematic errors in frequency differential magnetic induction tomography

H. Scharfetter

SFB-Report No. 2007–012 December 2007

A–8010 GRAZ, HEINRICHSTRASSE 36, AUSTRIA

Supported by the
Austrian Science Fund (FWF)

Der Wissenschaftsfonds.

SFB sponsors:

- **Austrian Science Fund** (FWF)
- **University of Graz**
- **Graz University of Technology**
- **Medical University of Graz**
- **Government of Styria**
- **City of Graz**

# Correction of systematic errors in frequency differential magnetic induction tomography

H. Scharfetter

Institute of Medical Engineering, Graz University of Technology, Kronesgasse 5, 8045 Graz, Austria

*Abstract*— **Frequency differential magnetic induction tomography allows the reconstruction of images of relative conductivity spectra with the aid of magnetic AC fields and coil arrays. While the technique works well at high frequencies (> 1 MHz) the induced voltages due to physiological conductivities are very low in the β-dispersion range of most tissues. Even when using special cancellation techniques for the primary magnetic field (e. g. gradiometers) the signals are sensitive to severe systematic errors. Small phase errors in the receiver network, thermal drift and small movements of the gradiometers can produce huge spurious signals which make image reconstruction very difficult. In this paper we propose a new method which allows for the cancellation of such errors in case of frequency differential MIT.**

*Keywords*— **Magnetic induction tomography, systematic errors,**

## I. Introduction

Magnetic induction tomography (MIT) has advanced considerably during the last decade and now the quality of MIT closely approaches that of EIT. However, the major disadvantage remain the very small signals which have to be extracted from a background of noise. At 100 kHz the ratio $\Delta V/V_0$ of the detected signal $\Delta V$ due to a conductivity change $\Delta\sigma$ and the voltage $V_0$ directly induced in the receiving coils can be as low as $10^{-6}$ -$10^{-7}$ for physiological conductivity changes in perturbations with a radius of few cm. $\Delta V/V_0$ is usually enhanced by a factor of around 1000 with gradiometers or zero-flow coils [1,2]. Here we focus on planar gradiometers for which typical arrangements are depicted in Fig. 1.

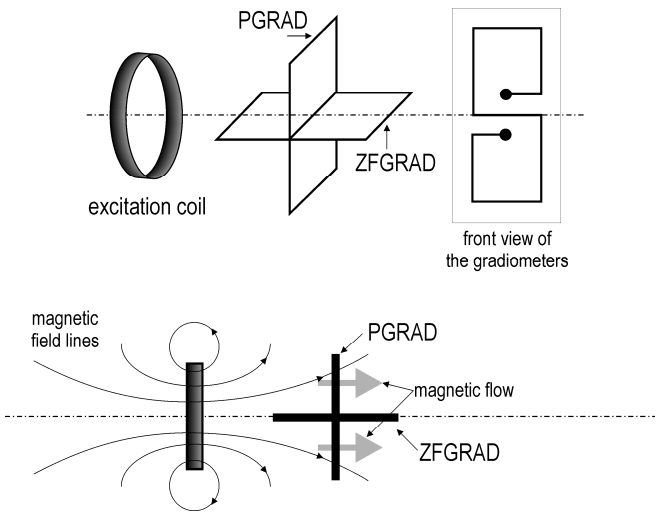


Fig. 1: possible orientations of planar gradiometers in the excitation field so as to achieve zero net magnetic flow. PGRAD: normal planar gradiometer, ZFGRAD: zero flow gradiometer [1]

As $\Delta V$ is 90° phase shifted with respect to $V_0$ it can be separated theoretically by coherent demodulation. However, small phase errors in the receiver network, e. g. due to thermal drift, project $V_0$ into the $\Delta V$ axis and thus produce huge spurious signals, for a detailed analysis see [3]. This leads essentially to three highly unwanted effects:

- Modulation of $\Delta V$ by a change of the projection angle (later denoted φ) due to thermal drifts of the gradiometer and the front end at a constant $V_0$
- Modulation of $\Delta V$ due to movements of the receiver coils with respect to the excitation coil (EXC) at a constant projection angle
- Modulation of $\Delta V$ due to metallic parts which move relatively to the coils and which change $V_0$ by changing the field geometry.

## II. Method and results

We propose a method which eliminates the above artefacts without the need for time-consuming and complicated calibration sequences. It is based on frequency-differential MIT (FDMIT), which exploits the fact that the frequency dependence of the conductivity of different tissues (ß-dispersion) depends on the specific type of tissue [4]. Thus a contrast between tissues can be obtained when measuring at different frequencies and subtracting the scaled signals.

### *A. Error model and error analysis*

Fig. 2 shows the equivalent network of the gradiometer coils plus the terminating network formed by the resistors $R_a$ and $R_a$'. The capacitances $C_a$ and $C_a$' denote the stray

Hermann Scharfetter, Robert Merva (Eds.): ICEBI 2007, IFMBE Proceedings 17, pp. 476–479, 2007

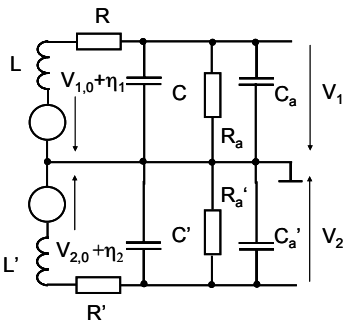


Fig. 2 : Equivalent gradiometer network.

capacitances of the preamplifiers. This network is the one published in [3] extended by the termination components.

The measurable voltages $V_1$ and $V_2$ are filtered copies of the induced EMFs which consist of the directly induced $V_{0,\#}$ and the signal voltages $\eta_{\#}$, whereby $\Delta V=\eta_1-\eta_2$. The transfer function for one half of the gradiometer is

$$H = \frac{1}{1+\frac{R}{R_a}-\omega^2 L(C+C_a)+j*\omega\left(R(C+C_a)+\frac{L}{R_a}\right)} \tag{1}$$

Sufficiently below the resonant frequency we can approximate this transfer function with a first order transfer function:

$$H_1 = \frac{1}{1+j*\omega\left(R(C+C_a)+\frac{L}{R_a}\right)} \tag{2}$$

For the following analysis we assume perfectly matched gradiometer halves provided that both have the same temperature. In case of a thermal mismatch, the values R, L, C differ from R', L', C' due to their thermal coefficients. In this case we get slightly different transfer functions $H_1$ and $H_2$ for both halves. With $|H_2|/|H_1| = a$ we can write:

$$H_1(\omega) = \frac{1}{1+j\omega\left(R(C+C_a)+\frac{L}{R_a}\right)} = |H_1|e^{j\varphi(\omega)}$$
$$H_2(\omega) = \frac{1}{1+j\omega\left(R'(C'+C_a')+\frac{L'}{R_a'}\right)} = |H_1|a(\omega)e^{j(\varphi(\omega)+\chi(\omega))} \tag{3}$$

$\chi$ is the phase difference between the two halves. For weak coupling the signal voltage $S = V_1 - V_2$ is [4]:

$$S(\omega) = j\omega\left(K_1H_1(\omega)-K_2H_2(\omega)\right) - \omega^2\left(K_3H_1(\omega)-K_4H_2(\omega)\right)\sigma(\omega) \tag{4}$$

The first term represents the difference of the two directly induced voltages $V_{0,\#}$ after filtering with the transfer functions $H_1$ and $H_2$, respectively. $K_1$, $K_2$ are the product of the excitation current and the mutual inductances between EXC and the gradiometer halves. The second righthand term denotes the signals $\eta_1$ and $\eta_2$. They are proportional to the perturbation's conductivity, the square of the frequency and coupling constants $K_3$ and $K_4$ which depend on the location and shape of the perturbation. For a fixed position and shape we may relate them by $K_4=cK_3$. Ideally $K_1$ and $K_2$ are equal in a completely balanced gradiometer. In real life they will differ by a factor b close to unity according to $K_2=bK_1$. Now we can re-write eq. (4):

$$S(\omega) = j\omega K_1|H_1(\omega)|\left(1-abe^{j\chi(\omega)}\right)e^{j\varphi(\omega)} + \omega^2K_3|H_1(\omega)|\left(1-ace^{j\chi(\omega)}\right)e^{j\varphi(\omega)}\sigma(\omega) \tag{5}$$

In the ideal case $H_1=H_2=1$ the first term at the right hand side becomes purely imaginary while the second one is purely real. The term $\omega^2K_3(1-ac)$ is the sensitivity of the idealized coil system to a perturbation. Evaluating only the real part allows a clear separation of the wanted signal from the carrier $V_{0,\#}$. In real life the transfer functions differ from unity. The phase error $\varphi(\omega)$ can be calibrated e. g. by measuring the frequency response of purely paramagnetic material. Multiplication with $e^{-j\varphi(\omega)}$ yields a corrected signal

$$\widetilde{S}(\omega) = j\omega K_1|H_1(\omega)|\left(1-abe^{j\chi(\omega)}\right) + \omega^2K_3|H_1(\omega)|\left(1-ace^{j\chi(\omega)}\right)\sigma(\omega) \tag{6}$$

$$\mathrm{Re}(\widetilde{S}(\omega)) = \omega K_1|H_1(\omega)|ab\sin\chi(\omega) + \omega^2K_3|H_1(\omega)|\left(1-ac\cos\chi(\omega)\right)\sigma(\omega) \tag{7}$$

Subtracting the ideal signal $\omega^2K_3(1-ac)\sigma(\omega)$ we get the absolute error:

$$E(\omega) = |H_1(\omega)|\omega K_1ab\sin\chi(\omega) + \omega^2K_3\left(|H_1(\omega)|-1-|H_1(\omega)|ac\cos\chi(\omega)+ac\right)\sigma(\omega) \tag{8}$$

Usually the phase mismatch between the two gradiometer halves can be assumed as very low, $|H_1(\omega)|$ is close to unity and $\omega^2K_3\sigma << \omega K_1$ so that the second right hand term is negligible with respect to the first one and the error can be approximated well enough with:

$$E(\omega) \approx \omega K_1|H_1(\omega)|ab\sin\chi(\omega) \tag{9}$$

Recognizing that for a PGRAD

$$\xi = \frac{\omega^2 K_3 (1 - ac)\sigma(\omega)}{\omega K_1} \tag{10}$$

is in the order of $10^{-6}$ to $10^{-7}$, the error term can easily come into the range of the ideal signal even at a very low $\chi$.

Now we expand the preceding analysis to the frequency differential case. A frequency-differential signal FSD can be obtained by weighting the individual components with the square of the frequency [5]:

$$FSD(\omega_1, \omega_2) = \left\{ \tilde{S}(\omega_1) - \left(\frac{\omega_1}{\omega_2}\right)^2 \tilde{S}(\omega_2) \right\} \tag{11}$$

For a further analysis we retain only the real part RFSD:

$$RFSD(\omega_1, \omega_2) = \mathrm{Re}\left\{ \tilde{S}(\omega_1) - \left(\frac{\omega_1}{\omega_2}\right)^2 \tilde{S}(\omega_2) \right\} \tag{12}$$

If we expand this further we get

$$\begin{aligned} &RFSD(\omega_1, \omega_2) = \\ &-\omega_1 K_1 \begin{Bmatrix} |H_1(\omega_1)| a(\omega_1) b \sin\chi(\omega_1) \\ -\frac{\omega_1}{\omega_2} |H_1(\omega_2)| a(\omega_2) b \sin\chi(\omega_2) \end{Bmatrix} \\ &+\omega_1^2 K_3 \begin{Bmatrix} |H_1(\omega_1)| (1 - a(\omega_1) c \cos\chi(\omega_1)) \sigma(\omega_1) \\ -|H_1(\omega_2)| (1 - a(\omega_2) c \cos\chi(\omega_2)) \sigma(\omega_2) \end{Bmatrix} \end{aligned} \tag{13}$$

Changes of the real part of the conductivity are reflected in the real part RFSD, while many error signals, such as vibrational signals, appear in the imaginary part [3].

Ideally ($H_1$=$H_2$=1) the first bracketed right term vanishes:

$$\begin{aligned} &RFSD_{ideal}(\omega_1, \omega_2) = \omega_1^2 K_3 (1 - c)(\sigma(\omega_1) - \sigma(\omega_2)) \\ &= \omega_1^2 K_3 (1 - c) \Delta\sigma \end{aligned} \tag{14}$$

whereby $\Delta\sigma$ is the difference of the conductivities at the two frequencies. This is the ideal weighted frequency-differential, being proportional to the difference of the conductivities at different frequencies. Again leaving out small terms we obtain as approximate error the difference of (13) and (14):

$$ESD(\omega_1, \omega_2) \approx \omega_1 K_1 \begin{Bmatrix} |H_1(\omega_1)| a(\omega_1) b \sin(\chi(\omega_1)) \\ -\frac{\omega_1}{\omega_2} |H_1(\omega_2)| a(\omega_2) b \sin(\chi(\omega_2)) \end{Bmatrix} \tag{15}$$

This is an offset term which corrupts the data for image reconstruction. In contrast to dynamic imaging, where the offset value is theoretically completely subtracted if the drift between two acquisitions is negligible, here no complete suppression can be achieved.

*B. nulling condition for the error signals*

A way out is to modify eq. (12) by correcting the frequency weighting factor with a correction $\gamma$ so that the bracketed expression in eq. (15) vanishes:

$$FSD(\omega_1, \omega_2) = \left\{ \tilde{S}(\omega_1) - \gamma \left(\frac{\omega_1}{\omega_2}\right)^2 \tilde{S}(\omega_2) \right\} \tag{16}$$

Re-analyzing the problem this way we obtain:

$$\begin{aligned} &RFSD_{CORR}(\omega_1, \omega_2) = \\ &-\omega_1 K_1 \begin{Bmatrix} |H_1(\omega_1)| a(\omega_1) b \sin\chi(\omega_1) \\ -\gamma \frac{\omega_1}{\omega_2} |H_1(\omega_2)| a(\omega_2) b \sin\chi(\omega_2) \end{Bmatrix} \\ &+\omega_1^2 K_3 \begin{Bmatrix} |H_1(\omega_1)| (1 - a(\omega_1) c \cos\chi(\omega_1)) \sigma(\omega_1) \\ -\gamma |H_1(\omega_2)| (1 - a(\omega_2) c \cos\chi(\omega_2)) \sigma(\omega_2) \end{Bmatrix} \end{aligned} \tag{17}$$

Subtracting the ideal signal (14) from (17) and again neglecting small terms in the second bracket yields the error:

$$\begin{aligned} &ESD_{CORR} \approx \\ &\omega_1 K_1 b \begin{Bmatrix} |H_1(\omega_1)| (a(\omega_1) \sin(\chi(\omega_1))) \\ -\gamma |H_1(\omega_2)| \frac{\omega_1}{\omega_2} (a(\omega_2) \sin(\chi(\omega_2))) \end{Bmatrix} \\ &+\omega_1^2 K_3 (1 - c)(1 - \gamma)\sigma(\omega_2) \end{aligned} \tag{18}$$

The first term reflects highly unwanted motion artefacts in case that b varies with time. It can be cancelled if

$$\gamma = \frac{|H_1(\omega_1)| (a(\omega_1) \sin(\chi(\omega_1)))}{|H_1(\omega_2)| (a(\omega_2) \sin(\chi(\omega_2)))} \frac{\omega_2}{\omega_1} \tag{19}$$

The second term in (18) is only a virtually static bias of the wanted differential signal, so it does not change with time. Defining as the wanted information the difference $\sigma(\omega_1)-\sigma(\omega_2)$ we can calculate the relative error:

$$e_r = \frac{(1 - \gamma)\sigma(\omega_2)}{(\sigma(\omega_1) - \sigma(\omega_2))} \tag{20}$$

Simulations show that sufficiently below the resonance frequency of the gradiometer $\gamma$ deviates from unity only by few percent, so that this bias may be acceptable and eq. 12 is still approximated sufficiently accurately.

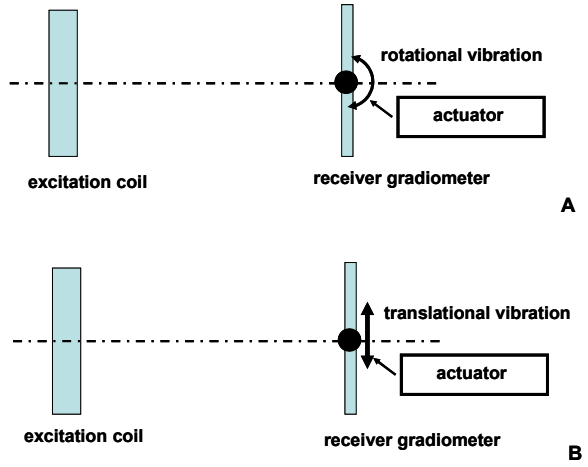


Fig. 3: possible mechanisms for modulating the signals by rotational (A) or translational (B) movements of the coils.

### *C. Method for achieving the nulling condition*

$\gamma$ can be determined experimentally for each frequency pair and for each coil combination from measurement by vibrating with the coil so as to modulate b and hence the true real part of the signal. The appropriate $\gamma$ is found when the modulation of the RFSD, i. e. the first right-hand term in eq. (17) disappears. A mechanical modulation of the coil can be introduced in different ways. Two examples are shown in Fig. 3.

## III. Discussion

We have derived a method for cancelling systematic errors in multi-frequency MIT which are due to phase errors in the measurement channels and gradiometers. The correction factor $\gamma$ guarantees that any projections of imaginary EMFs are projected into the real axis and hence all motion artefacts disappear. At the same time thermal drift problems of the transfer functions are solved, because the nulling factor can be adapted continuously. Assessing eq. (17) in detail shows that the modulation depends on two factors, i. e. changes of the coil's misalignment, described by b(t) and changes of the coupling, described by $K_1(t)$. The first is responsible for movement artefacts in conjunction with phase errors, the second one for alterations of the mutual coupling between exciters and receivers. One important source for the second factor is the presence of metallic parts near the coils, which can produce significant artefacts [3]. Conductors with high conductivity behave like coupled inductor coils which therefore essentially modify the coupling $K_1$. The nulling procedure therefore also cancels these contributions.

## Acknowledgment

This work was supported by the SFB project F32-N18 granted by the Austrian Science Fund.

## References

1. Scharfetter H, Merwa R, and Pilz K (2005) A new type of gradiometer for the receiving circuit of magnetic induction tomography (MIT). Physiol Meas 26: S307–S318
2. Watson S et al. (2004) A primary field compensation scheme for planar array magnetic induction tomography. Physiol Meas 25: 271–279
3. Scharfetter H, Casañas R, Rosell (2003) J Biological tissue characterization by magnetic induction spectroscopy (MIS): requirements and limitations. IEEE Trans Biomed Eng 50: 870-880
4. Gabriel S, Lau RW, Gabriel C 1996 The dielectric properties of biological tissues: III. Parametric models for the dielectric spectrum of tissues. Phys. Med. Biol. 41, 2271-93, 1996
5. Brunner P, Merwa R, et al (2006) Reconstruction of the shape of conductivity spectra using differential multi-frequency magnetic induction tomography. Physiol Meas 27: S237–S248

Address of the corresponding author:

Author: Hermann Scharfetter
Institute: Inst. Of Medical Engineering
Street: Kronesgasse 5
City: Graz
Country: Austria
Email: hermann.scharfetter@tugraz.at